Flood Vulnerability and Climate Adaptation of Maritime Built Heritage in Historic Shimoni Town, Southern Kenya Coast

Wallace Njiiri[1*], Mugwima Njuguna[1] & Ephraim Wahome[2]

[1]*Department of Architecture, Jomo Kenyatta University of Agriculture and Technology, Nairobi, Kenya (njiirikihiko@gmail.com)*

[2]*Department of Landscape Architecture, Jomo Kenyatta University of Agriculture and Technology, Nairobi, Kenya (mugwima@gmail.com)*

[3]*Department of History and Archaeology, University of Nairobi, Kenya (ewahome@uonbi.ac.ke)*

**Corresponding author: njiirikihiko@gmail.com*

https://doi.org/10.62049/jkncu.v6i2.559

Abstract

Coastal Kenya records the highest incidence of marine heatwaves in the western Indian Ocean basin, intensifying rainfall and flooding of historic monuments, buildings and archaeological sites. Despite growing concern over climate-related flooding in historic settlements, flood vulnerability assessment remains limited in Kenya. This study applied geospatial analysis to assess flood vulnerability in historic Shimoni Town using satellite imagery and Digital Elevation Models (DEM). Slope, elevation, flow accumulation, drainage density, Topographic Wetness Index (TWI), Topographic Position Index (TPI), and vegetation cover (NDVI) were integrated within a GIS-based Flood Hazard Index across the 40 km² study area. Limited hydrological datasets and flood inventories constrained calibrated weighting approaches; therefore, a linear combination method was adopted and validated through field observations, transect walks and expert consultations. Very gentle slopes (0–2.3°) contributed 44.11% of flood risk despite covering only 3.62% of the area. Low elevations contributed 28.82% of flood risk, while high drainage density (28.76%), high TWI (27.41%), low TPI depressions (27.34%), and high flow accumulation (26.33%) intensified flooding within low-lying zones. High NDVI zones (0.45–0.51) recorded high flood risk (21.67%), indicating that vegetation alone cannot offset unfavorable terrain and hydrological conditions. Highly susceptible areas included colonial headquarters, cemeteries, mosque ruins, jetties, and ritual cave entrances, whereas sacred Kaya forests, baobab and fig tree groves exhibited lower susceptibility. Findings show that flood vulnerability extends beyond individual monuments to interconnected hydrology–heritage systems, supporting recommended long-term watershed management, ecological restoration, planned retreat, and urgent interventions including contour drains, vegetated swales, permeable paving, and early warning systems. The study advances heritage climatology and represents the first DEM-based Flood Hazard Index application for maritime built heritage adaptation in Kenya.

Keywords: Maritime Built Heritage, Flood Vulnerability, Adaptation, Conservation, Southern Kenya Coast

Built Heritage and Flood Vulnerability

Floods are among the most unpredictable climate-driven disasters and account for one-third of damage to built heritage caused by all natural hazards globally (Salazar et al., 2024). In coastal regions, flooding is increasingly intensified by sea level rise and extreme rainfall associated with warmer sea surface temperatures (Reimann et al., 2018). Coastal Kenya is particularly vulnerable because it records the highest incidence of marine heatwaves in the western Indian Ocean (WIO) basin (Saranya et al., 2022), while mean sea surface temperatures have risen to 1.28°C at a rate of 0.1°C per decade (Njiiri et al., 2025). Consequently, historic settlements such as Faza (Plate 1) and Kizingitini along the northern coast, have experienced recurrent flooding linked to extreme rainfall events (Hamza et al., 2020; De Jesus Neto, 2023; Kazungu, 2020; 2024). Existing studies further demonstrate that historic materials commonly used in coastal Kenya, including palm thatch, coral rag, timber, and wattle-daub, are highly vulnerable to salt crystallization, biological growth and moisture-related deterioration (Njiiri et al., 2024; Gitau et al., 2025).

Plate 1: Flooding in Faza, Pate Island (Source: Kazungu, 2024)

Notably, water is the most important decay factor in historic environments (Sesana et al., 2019). Longer periods of wetness, together with higher temperatures, create favourable conditions for decay by fungi, algae, mold, and pests, resulting in the loss of familiar landscapes (Cook et al., 2019). The development of lichens' thalli, the vegetative tissue of lichens, results in biomass accumulation, solubilisation, and de-cohesion of mineral grains (Blavier et al., 2023). Furthermore, corrosion, a chemical process that deteriorates materials through the erosive action of water and salt deposition, is more prevalent in the presence of extreme rainfall (Iosub, 2019; Appiotti et al., 2020).

In coastal Kenya, the dissolution of salts caused by recurrent wetting and drying results in the blackening of historic monuments, as observed at Siyu Fort on Pate Island (Plate 2) and Fort Jesus in Mombasa old town (Plate 3). Overall, flood-related damage to maritime built heritage can be permanent or extremely difficult to restore, while losses in historical, archaeological, and aesthetic value reduce visitor satisfaction and cause economic decline (Arrighi, 2021; Kotova et al., 2023). Therefore, urgent flood mitigation measures are necessary in historic environments to prevent further deterioration of cultural property.

Plate 2: Surface blackening, Siyu Fort (Source: Njiiri et al.,2025a)

Plate 3: Surface blackening, Fort Jesus, (Source : Njiiri et al.,2024)

Although flood hazard mapping has increasingly been applied in historic environments in Ethiopia, Algeria, Somalia, and Egypt (Abay et al., 2019; Osman & Das, 2023; Khalil et al., 2022; Maou et al., 2025; Allam et al., 2025), comparable studies remain absent along Kenya's coast despite the existence of sixty-six littoral historic sites exposed to rising sea levels, shoreline erosions and tidal inundation (Njiiri et al., 2025a). Current flood management practices by local agencies continue to rely on outdated approaches such as watermarks, field observations, aerial reconnaissance, and media reports (GoK, 2019; Mwakumanya, 2021; Cece, 2024). Moreover, emerging anthropogenic pressures, including mineral exploration, logging, sand extraction, groundwater abstraction, and port development, increasingly alter drainage systems and intensify runoff within historic settlements (Hamza et al., 2020; Kilaka & De Jesus Neto, 2023; Oyugi, 2021).

Fortunately, heritage climatology identifies flood factors that are effective in determining flood vulnerability (Brimblecombe et al., 2024). These factors are derived from variations in elevation (Mabrouk et al., 2022; Tascón-González et al., 2024) and hydrologic parameters (Adnan et al., 2019; Khalifa et al., 2022) used in flood risk assessment (Alqahtani & Qaddah, 2019). The flood causative factors include slope, aspect, elevation, profile curvature, drainage density, flow accumulation, depth of fragmentation, topographic wetness index, topographic position index, stream power index, and sediment transport index (Bashir, 2023; Bonazza et al., 2023; Ashfaq et al., 2025; Haou et al., 2025; Hanwat & Tripathi, 2025). However, these methods have not been systematically applied to heritage conservation planning in Kenya.

To address existing research gaps, this study investigates flood vulnerability in historic Shimoni Town by evaluating the role of flood hazard mapping in climate adaptation and heritage conservation. As one of the first studies of its kind on the Kenyan coast, the research advances theoretical scholarship in heritage climatology by linking flood vulnerability with settlement morphology within a coastal heritage context. Methodologically, it introduces a novel application of a DEM-based Flood Hazard Index integrating hydrological and topographic indicators to assess built heritage vulnerability in coastal Kenya.

From a heritage practice and policy perspective, the study provides an evidence-based spatial framework to support climate adaptation, heritage-sensitive zoning and prioritization of vulnerable heritage assets for urgent conservation intervention. The findings reinforce international evidence that topographic and hydrological variables strongly shape flood vulnerability (Wahba et al., 2023; Taib et al., 2024; Mohammed et al., 2024; Cacciotti et al., 2024), while demonstrating that the interaction between climate hazards, settlement pattern and heritage distribution remains poorly understood within Kenya's historic settlements.

Historic Shimoni Town and Flood Vulnerability

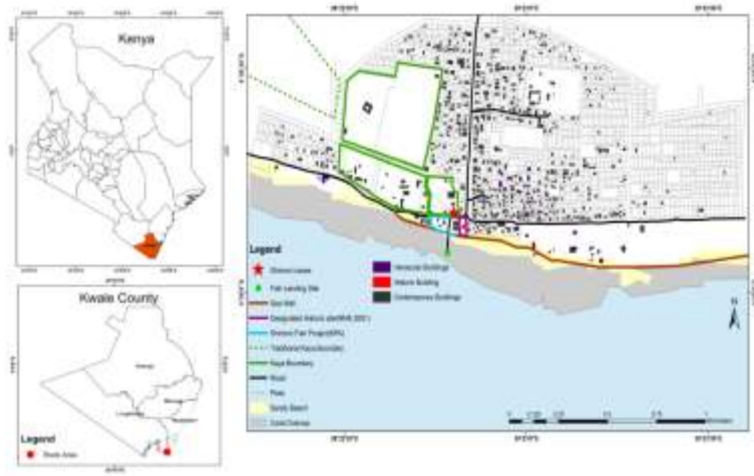

Figure 1: Kenya Coast (Source: Authors, 2026)

Shimoni town is located 90 kilometres south of Mombasa on a peninsula 13 kilometres from the Mombasa Lunga Lunga route near the Kenya-Tanzania border, Kwale County; 4.6471° S, 39.3805° E (Figure 1).

Shimoni lies within the Inter-Tropical Convergence Zone (ITCZ), a key element of the Earth's climate system (GoK, 2019). This unique wind reversal pattern influences precipitation patterns across the 3 km-wide Shimoni strait. However, high-intensity rainfall compounds different patterns of decay for designated historic assets, including British colonial headquarters built in 1884 (Plate 5), colonial prisons built in 1886 (Plate 6), colonial armouries, cemeteries, wells and jetties. Traditional building materials, including coral, timber, and lime plaster, undergo frequent splitting, cracking, and mould proliferation, accelerated by high-intensity rainfall and frequent flooding (Busaka et al., 2023; Njiiri et al., 2024).

Local traditional house forms (Plates 7 and 8), assembled with palm thatch, wattle-daub, and coral rag, are easily damaged during extreme rainfall events. In particular, palm thatch, locally known as makuti, is increasingly prone to termite attack, necessitating costly replacements. Furthermore, periodic flooding creates a conducive environment for pest infestation and the growth of invasive species that detract from aesthetic value. These species include Vachellia reficiens, Prosopis juliflora, Lantana camara, Azadirachta indica, and Pedilianthus tithymaloides (Betts et al., 2019; Cazalis et al., 2022).

Overall, perennial flooding across the heritage landscape has been linked to periods of high humidity that follow abnormally long rains associated with El Niño-Southern Oscillation events (Wainwright et al., 2019; Njiiri et al.,2025). For archaeology yet to be uncovered, the lloss of stratigraphic integrity due to cracking and heaving caused by changes in sediment moisture is on the rise (Njiiri et al., 2024). This is the case for bburied archaeology, including Kyangai Mosque (Kusimba, 2004) and the ancient settlement of Kichangani in the western portion of historic Shimoni town (Kiriama, 2017).

Plate 5: British Colonial Headquarters (Source: Njiiri et al.,2024)

Plate 6: British Colonial Prisons (Source: Njiiri et al.,2024)

Plate 7: Traditional wattle-daub building (Source: Authors, 2025)

Plate 8: Traditional coral rag building (Source: Authors, 2025)

Methodology

To better target climate adaptation, the methodology described below was designed to assess flood vulnerability in historic Shimoni town on the southern Kenya coast. This aimed to provide a baseline for prioritizing conservation strategies that enhance capacities to mitigate flooding events. To obtain high-resolution topographic data, slope, elevation, topographic wetness index, topographic position index, flow accumulation, and drainage density were derived from a Digital Elevation Model (DEM), while land cover was extracted using the Normalized Difference Vegetation Index (NDVI) generated from satellite imagery (Table 1).

Table 1: Sources of Data

Parameter	Flood Variable	Data Description	Source
Topography	Slope, Elevation	DEM: Version 3, spatial resolution 30m	Shuttle Radar Topography Mission (SRTM 1 arc-second, USGS) https://search.earthdata.nasa.gov/
Hydrology	Topographic Wetness Index, Topographic Position Index, Flow Accumulation, Drainage Density,		
Land cover	Normalized Difference Vegetation Index (NDVI)	Landsat 8: High-resolution 10 m × 10 m	Operational Land Imager and Thermal Infrared Sensor

A Digital Elevation Model (DEM) specifies the elevation of any point in a particular area at a spatial scale (Chowdhury, 2023; Tanrıverdi & Ayaşlıgil, 2026). A key element of this approach was the use of Shuttle Radar Topography Mission (SRTM) data, obtained from the USGS Earth Explorer (Burshtynska et al., 2023; Amellah et al., 2024). The dataset, captured in March 2026, provided a Digital Elevation Model (DEM) at 30-m resolution, offering detailed, reliable elevation data essential for the accurate extraction of flood-causing factors.

However, digital elevation models contain topographic depressions that take the form of either single-cell pits or contiguous areas (Ahmad et al., 2025). Prior to analysis, several pre-processing steps were applied to the DEM. These include mosaicking to maintain a seamless elevation model and resampling to harmonize hydrological conditioning (Jiang et al., 2022; Xafoulis et al., 2023). The final DEM was then clipped to the study area boundaries using the Fill tool in ArcGIS 10.8. To ensure consistency with other spatial datasets, the DEM tiles were projected to the WGS 84 / UTM Zone 36N coordinate system. The stepwise sequence for data acquisition, mosaicking, resampling, and projection by the Universal Transverse Mercator (UTM) projection system is illustrated in Figure 1.

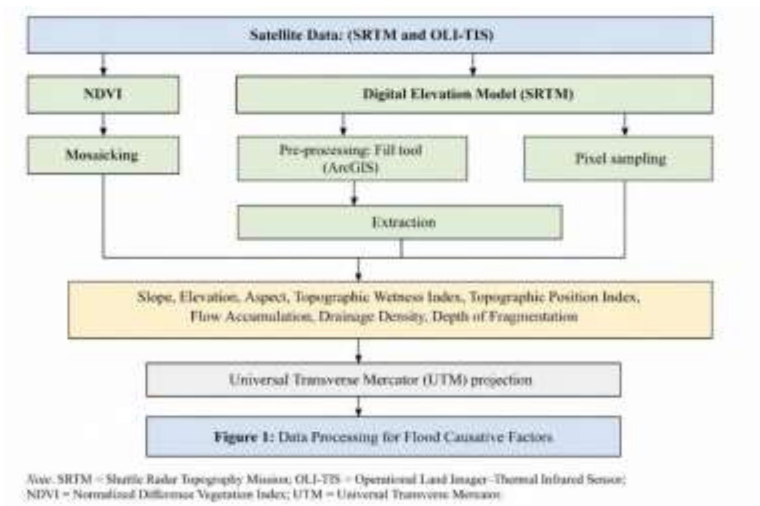

Figure 2: Data Processing for Flood Causative Factors (Source: Authors, 2026)

Slope

Slope, defined as the ratio of elevation change to horizontal distance between two points, is a key factor in evaluating land loss from inundation (Zhang et al., 2025). As the slope angle increases, infiltration processes and velocity-driven erosion intensify (Zhang et al., 2021). Thus, slope shows an inverse relationship with flood potential, with flatter regions posing a higher risk of water accumulation (Neto & Carr, 2021). The arctangent function in the Spatial Analyst extension of ArcGIS 10.8 was used to obtain slope angle values using Equation 1.

$$S^{\circ} = \arctan\left(\sqrt{(dz/dx)^2 + (dz/dy)^2}\right) * (180 / \pi) \quad \text{(Equation 1)}$$

Where S° is the slope in degrees, dz/dx and dz/dy represent the change in elevation (z) with respect to changes in the x and y coordinates, respectively (Zhang & Liu, 2022).

Elevation

Elevation, the height of a point above mean sea level, plays an important role in the direction of high-magnitude floods (Guth et al.,2021). Different elevations alter climate characteristics, leading to differences in soil moisture that affect drainage characteristics (Boulton & Stokes, 2018). Notably, flood risk increases with decreasing elevation; hence, areas of low elevation are more vulnerable to flooding (Tran et al., 2022). To obtain elevation point data, grid cell values from the Digital Elevation Model were extracted using the mapping tool in ArcGIS 10.8.

Topographic Wetness Index

The topographic wetness index is a morphometric proxy for soil moisture derived from the topographic condition of a basin unit (Liang & Chan, 2017). Soil moisture is predicted from the proxy to establish aridity, vegetation seasonality, and ecosystem modelling (Kopecký et al., 2020). Regions with higher values are expected to be moister than those with lower scores (Slezák et al., 2022). The topographic wetness index is calculated using local slope angle and the upslope area that flows through each point per unit contour length (Różycka et al., 2017). The index was computed using a DEM as input data in the Basic Terrain Analysis of SAGA GIS 7.9, using Equation 2.

$$TWI = \ln (a / \tan(b)) \quad \text{(Equation 2)}$$

Where TWI refers to the topographic wetness index, a represents the upslope contributing area (m^2) derived from flow accumulation, and b is the local slope angle in degrees.

Topographic Position Index

The topographic positioning index (TPI) quantifies the elevation difference between a cell and its neighbours (Lee & Rezaie, 2022). It reflects the tendency of water to accumulate at a specific location or to flow downward under gravity (Al-Sababhah, 2023). The index compares the altitude of a particular cell with the mean altitude of the neighbourhood around that cell. A positive TPI indicates a ridge above the neighbourhood average, while a negative TPI indicates a valley below the neighbouring cells (Habib, 2021). Values near 0 indicate a constant slope; if the slope is significantly greater than 0, the region is steep, and if the slope is close to 0, the region is flat (Neoga et al., 2025). The Topographic Position Index was computed using a DEM as input data in the Basic Terrain Analysis of SAGA GIS 7.9, using Equation 3.

$$TPI = CV - Mcn \quad \text{(Equation 3)}$$

Where TPI refers to the Topographic Position Index, CV is the elevation value of the central cell in the Digital Elevation Model, and Mcn is the average elevation of the cells within a defined radius around the central cell (Asrade et al., 2026).

Flow Accumulation

Flow accumulation is a strong indicator of where runoff from larger upslope areas converges (Zhang & Liu, 2022). This indicator represents the number of upstream cells that contribute runoff to a particular location in a Digital Elevation Model (DEM) (Shuaibu et al., 2022). Low accumulation values are found in areas of lower-order streams, and higher values are found at the confluences of higher-order streams (Bello et al., 2024). The index is used to identify the most advantageous locations for soil-protection features, such as gabions and cut-off drains (Basu et al., 2023). Flow direction was extracted from the DEM, with each cell's value indicating the direction towards which water would flow.

Drainage Density

Drainage density is defined as the total length of waterways in a basin divided by the basin's area (Dragičević et al., 2019). Higher drainage density increases the likelihood and severity of flash floods. Lower drainage density slows runoff, reducing flood peaks (Gao et al., 2022). Thus, areas of low drainage density have a lower likelihood of flooding, whereas areas of high drainage density have a greater likelihood of flooding (Xiong & Wang, 2022). To prepare a drainage density map of the study area, stream order was extracted from the DEM using the line density tool in ArcGIS 10.8 with Equation 4.

$$\text{Drainage density (Dd)} = \sum_{i=1}^{i=n} * \text{ Di /A (km}^{-1}\text{) (Equation 4)}$$

Where ∑Di is the total length of the stream in the grid (km), and *A* is the grid area (km^2).

Normalized Difference Vegetation Index

The Normalized Difference Vegetation Index (NDVI) is a measure of vegetation cover that helps determine permeability and infiltration rates (Ikirri et al., 2022). Densely vegetated areas support the percolation of extreme rainfall, whereas built-up areas support overland flow (Xu et al., 2018). Positive NDVI values indicate active vegetation; values close to zero represent barren areas, while negative values refer to water bodies (Xiong & Wang, 2022). Thus, a decrease in NDVI is considered to increase flood vulnerability (Bishikwabo et al., 2025). The Normalized Difference Vegetation Index was computed using Equation 5.

$$\text{NDVI} = [(\text{NIR} - \text{R}) / (\text{NIR} + \text{R})] \text{ (Equation 5)}$$

Where NIR refers to the reflected light in the near-infrared portion of the electromagnetic spectrum. R refers to the reflected light in the visible red portion of the electromagnetic spectrum (Ikirri et al., 2022; Mishra et al., 2022).

Overall, the nine flood-causative factors were aggregated to map flood vulnerability in historic Shimoni town. Quantitative categories for each factor were assigned numerical values using the Natural Breaks (Jenks) classification method implemented in ArcGIS 10.8. The method was preferred over equal interval and quantile classification because it minimizes intra-class variance while maximizing inter-class differences, thereby improving the representation of naturally occurring spatial groupings within environmental datasets (Cacciotti et al., 2024; Shrestha et al., 2025; Pimenta et al., 2025). Similar GIS-based flood vulnerability studies have demonstrated that Natural Breaks classification improves the spatial differentiation of flood-prone terrain in heterogeneous coastal landscapes (Alqahtani & Qaddah, 2019; Wahba et al., 2023; Devi et al., 2025; Haou et al., 2025; Zhao et al., 2026).

To establish the Flood Hazard Index (FHI), the final raster overlay was classified into five categories: Very Low (1), Low (2), Moderate (3), High (4), and Very High (5) using a linear combination approach shown in Equation 6 (Elsebaie et al.,2023; Sajid et al., 2025).

$$\text{FHI} = \text{S} + \text{E} + \text{TWI} + \text{TPI} + \text{F} + \text{Dd} + \text{NDVI} \text{ (Equation 6)}$$

Where S is slope, E is elevation, TWI is topographic wetness index, TPI is topographic position index, F is flow accumulation, Dd is drainage density and NDVI is Normalized Difference Vegetation Index (Ashfaq et al., 2025; Alba-Fernández et al., 2021; Tascón-González et al., 2024; Hanwat & Tripathi, 2025; Maou et al., 2025; Allam et al., 2025).

Methodological Justification

The linear combination method was adopted because it provides a transparent and reproducible approach for integrating multiple spatial variables while minimizing subjective expert-driven weighting biases (Cacciotti et al., 2024; Alafostergios et al., 2025). Equal weighting was considered appropriate since all selected variables are established determinants of runoff concentration, water retention, and surface inundation in flood hazard studies (Adnan et al., 2019; Bashir, 2023; Bonazza et al., 2023; Hanwat & Tripathi, 2025).

Notably, the absence of long-term hydrological datasets and flood inventories for historic settlements along the Kenya coast constrained the application of statistically calibrated methods. Further, Analytical Hierarchy Process (AHP) and machine learning approaches depend on expert judgment (Taib et al., 2024; Haou et al., 2025; Zhao et al., 2026), extensive flood records (Khalifa et al., 2022; Mohammed et al., 2024; Ashfaq et al., 2025) and large high-resolution datasets that remain unavailable in coastal Kenya (Njiiri et al.,2024;2025a). Consequently, the linear combination method was considered most suitable for exploratory flood vulnerability assessment in a data-scarce heritage environment.

Data Validity

Data validation was conducted through comparison of spatial outputs with field observations and expert consultations involving Shimoni heritage management staff and physical planners from the Kwale County Department of Natural Resources, Environment, and Urban Planning. Ground-truthing exercises including transect walks and visual inspections identified visible indicators of flood exposure, including eroded shorelines near coral buildings (Plate 9) and recurrent surface runoff around cave entrances and wattle-daub structures (Plate 10). The visual inspections corresponded closely with areas classified as high and very high flood susceptibility within the mapped Flood Hazard Index (FHI). Validation was further supported through comparison with documented flood-prone areas reported in historical accounts of flooding along the Kenya coast (Awuor et al.,2008; Johnson, 2013; Omuombo et al., 2013; Mwakumanya, 2021).

Limitations

Plate 9: Eroded shorelines near coral buildings (Source: Authors, 2026)

Plate 10: Damaged wattle-daub structures (Source: Authors, 2026)

Despite its usefulness, the Flood Hazard Index (FHI) contains several limitations. First, the index primarily relies on topographic and hydrological variables derived from DEM data and does not explicitly incorporate short-term meteorological variability such as rainfall intensity, tidal surges, wave action, or future sea-level rise scenarios. Second, equal weighting assumes uniform influence among variables even though some flood factors exert stronger effects under particular environmental conditions. Third, the spatial resolution of the DEM may not fully capture micro-topographic variations within densely built historic environments. Finally, limited availability of long-term flood inventories constrained the application of advanced statistical calibration and predictive accuracy assessment.

Uncertainty

Flood Hazard Index (FHI) uncertainty arises from potential DEM interpolation errors, seasonal hydrological fluctuations and the dynamic interaction between natural and anthropogenic processes affecting runoff patterns. Additional uncertainty results from changes in land use, shoreline modification, groundwater abstraction, and future climate variability that alters flood behavior over time (Hamza et al., 2020; Kilaka & De Jesus Neto, 2023; Devi et al., 2025; Zhao et al., 2026). Nevertheless, despite these uncertainties, the FHI provides a robust first-order spatial framework for identifying vulnerable zones and supporting climate adaptation planning in data-constrained coastal heritage landscapes.

Results and Interpretation

The Digital Elevation Model (DEM) provided reliable elevation data for extracting and integrating flood-causative factors grouped into terrain, hydrology, and surface condition variables. Terrain variables included slope and elevation, hydrological variables included flow accumulation, drainage density, topographic wetness index and topographic position index, while surface condition variables included the Normalized Difference Vegetation Index.

Terrain

Slope and elevation emerged as critical topographic controls influencing the spatial distribution of flood vulnerability in historic Shimoni town. The analysis demonstrates that gentler slopes between 0 and 2.3° exhibited the highest flood susceptibility, contributing 44.11% of the total flood risk despite covering only 3.62% (1.45 km²) of the study area (Table 2). These flatter eastern sections of the settlement promote slower surface runoff, prolonged ponding, and water retention during intense rainfall and high-tide flooding events (Figure 2). In contrast, steeper slopes ranging from 10.60° to 13.05° covered 39% (15.64 km²) of the total surface area, contributing a comparatively lower 10.96% of flood risk because rapid downslope runoff limits water accumulation. The findings confirm that slope functions as a first-order determinant of flood behavior by regulating runoff velocity and temporary water ponding across the historic landscape.

Table 2: Slope

Flood Factor	Subclass	Rank	Remark	Area (km²)	% of Total Area	Flood Area (km²)	% of Flood Area
Slope (°)	0 – 2.3	5	Very High	1.45	3.62	0.801	44.11
	2.3 – 4.9	4	High	12.01	30.03	0.519	28.58
	4.9 – 7.1	3	Moderate	10.66	26.64	0.141	7.76
	7.1 – 10.6	2	Low	0.24	0.62	0.156	8.59
	10.6 – 13.05	1	Very low	15.64	39.09	0.199	10.96
Total				40	100	1.816	100

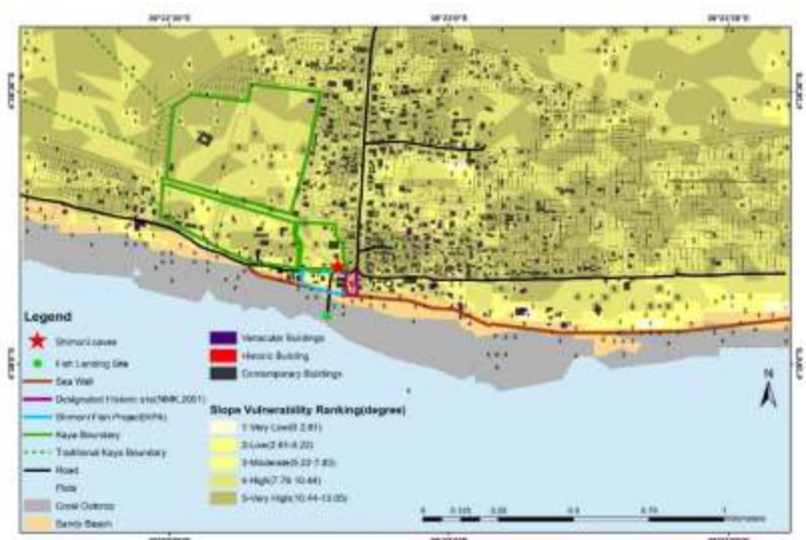

Figure 3: Slope (Source: Authors, 2026)

Elevation similarly played a significant role in controlling flood exposure and inundation patterns. Low-lying terrain between -5 and 1.8 m above mean sea level occupied 22.70% (9.08 km²) of the study area and contributed 28.82% of total flood risk due to increased accumulation of surface runoff (Table 3). Conversely, higher elevations between 18.30 and 28 m accounted for 14.21% (5.68 km²) of the study area and contributed 24.54% of flood risk because runoff naturally drains downslope under gravity. Consequently, northern plateau areas are less susceptible to flooding compared to low-lying shoreline zones and depressions (Figure 3).

Table 3: Elevation

Flood	Subclass	Rank	Remark	Area (km²)	% of Total	Flood Area	% of Flood
Elevation (m)	-5 – 1.8	5	Very High	9.08	22.70	0.807	28.82
	1.8 – 7.2	4	High	8.95	22.38	0.157	5.61
	7.2 – 12.6	3	Moderate	5.19	12.98	0.376	13.43
	12.6 – 18.3	2	Low	11.10	27.75	0.773	27.61
	18.3 – 28	1	Very low	5.68	14.20	0.687	24.54
Total				40	100	2.800	100

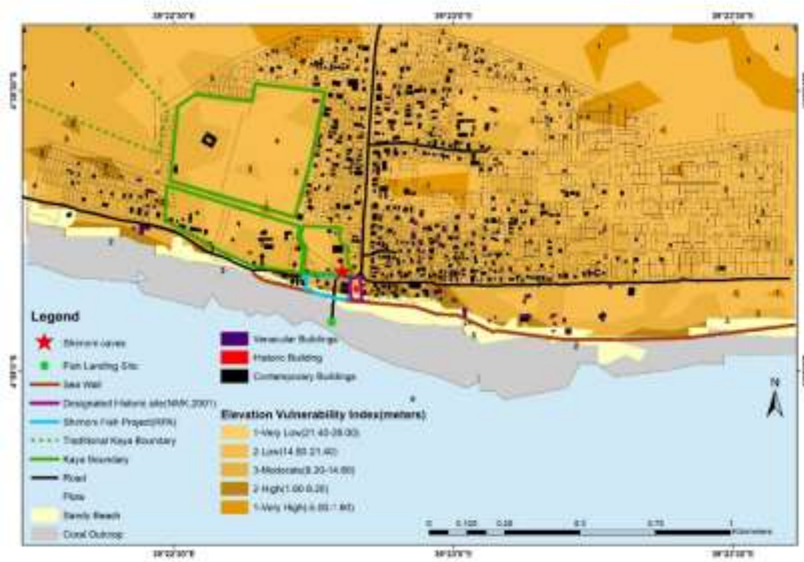

Figure 3: Elevation (Source: Authors, 2026)

From a heritage conservation perspective, low elevations and gentle slopes increase the flood vulnerability of coral-stone colonial buildings, mosque ruins, cemeteries, wells, jetties, and traditional residential compounds located within flood-prone terrain. Recurrent wetting and drying accelerate salt crystallization, mortar deterioration, biological growth, and structural weakening in coral stone structures, while wattle-and-daub buildings are vulnerable to wall slumping, floor erosion, and timber decay. The findings show that flood vulnerability in Shimoni affects the

wider settlement landscape rather than isolated monuments, highlighting the need for elevation-sensitive and landscape-scale conservation strategies focused on drainage improvement, runoff control and land-use regulation.

Hydrology

Hydrological variables, including flow accumulation, drainage density, topographic wetness index (TWI), and topographic position index (TPI), emerged as major determinants of flood vulnerability in historic Shimoni town. The variables directly influence soil saturation, drainage efficiency, and the spatial movement of floodwaters across the heritage landscape. Flow accumulation revealed the pathways through which runoff converges and concentrates within the settlement (Figure 4). High flow accumulation values ranging from 545.60 to 682 covered 12 km², representing 30% of the total study area, and contributed 26.33% of the total flood risk (Table 4). These high-flow corridors coincide with perennial drainage channels converging toward the designated historic site, particularly within low-lying eastern sections of the settlement. In contrast, low accumulation values ranging from 0 to 136.40 occupied only 2.83 km² (7.08%) and contributed 10.29% of flood risk.

Table 4: Flow Accumulation

Flood Factor	Subclass	Rank	Remark	Area (km²)	% of Total Area	Flood Area (km²)	% of Flood Area
Flow Accumulation	0 – 136.4	1	Very Low	2.83	7.08	0.334	10.29
	136.4 – 272.8	2	Low	8.08	20.2	0.592	18.25
	272.8 – 409.2	3	Moderate	8.51	21.28	0.677	20.87
	409.2 – 545.6	4	High	8.57	21.42	0.787	24.26
	545.6 – 682	5	Very high	12.01	30.02	0.854	26.33
Total				40	100	3.244	100

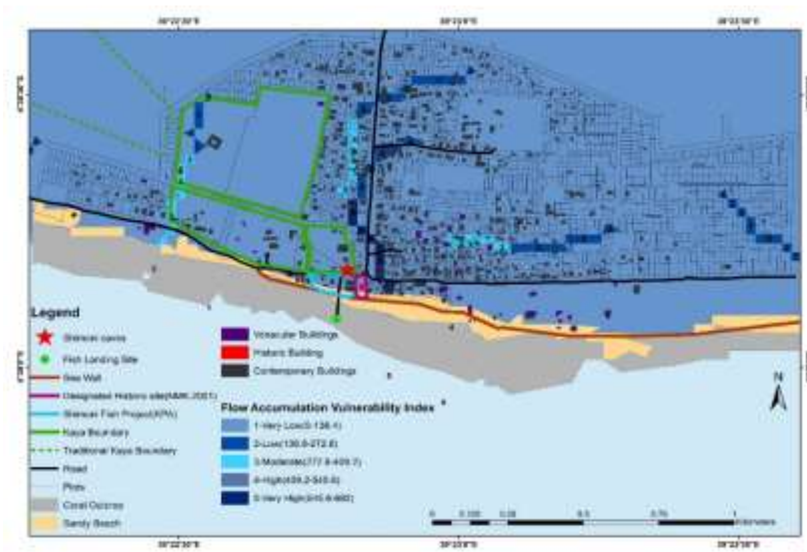

Figure 4: 4: Flow Accumulation (Source: Authors, 2026)

The findings indicate that areas with concentrated runoff pathways experience repeated water ponding, sediment deposition, and debris transfer during heavy rainfall events. From a heritage conservation perspective, this is particularly significant because colonial ruins, mosque remains, shrines, and historic compounds situated within these runoff corridors remain exposed to recurrent inundation and erosion processes.

The analysis therefore shifts conservation thinking from monument-centered protection toward catchment-scale hydrological management. Protecting heritage structures in isolation is unlikely to succeed if upstream runoff generated through road expansion and vegetation clearance continues to be directed toward vulnerable heritage zones. Consequently, flow accumulation analysis provides a strong basis for infiltration enhancement, runoff attenuation, and redesign of drainage infrastructure within the historic settlement.

Drainage density similarly played an important role in determining flood concentration and transfer within Shimoni town. High drainage density values ranging from 3,211 to 4,013 accounted for 9.28 km² (23.20%) of the total surface area and contributed 28.76% of total flood risk, while low drainage density values ranging from 0 to 802 occupied 6.13 km² (15.33%) and contributed only 3.84% of flood risk (Table 5). The concentration of dense drainage networks within the central historic core, characterized by compact wattle-and-daub settlements and limited open spaces, increases the likelihood of localized ponding and overflow along the north–south main street (Figure 5).

Table 5: Drainage Density

Flood Factor	Subclass	Rank	Remark	Area (km²)	% of Total Area	Flood Area (km²)	% of Flood Area
Drainage Density	0 – 802	1	Very Low	6.13	15.33	0.125	3.84
	802 – 1605	2	Low	7.97	19.92	0.555	17.03
	1605 – 2408	3	Moderate	8.06	20.15	0.762	23.39
	2408 – 3211	4	High	8.56	21.4	0.879	26.98
	3211 – 4013	5	Very high	9.28	23.20	0.937	28.76
Total				40	100	3.258	100

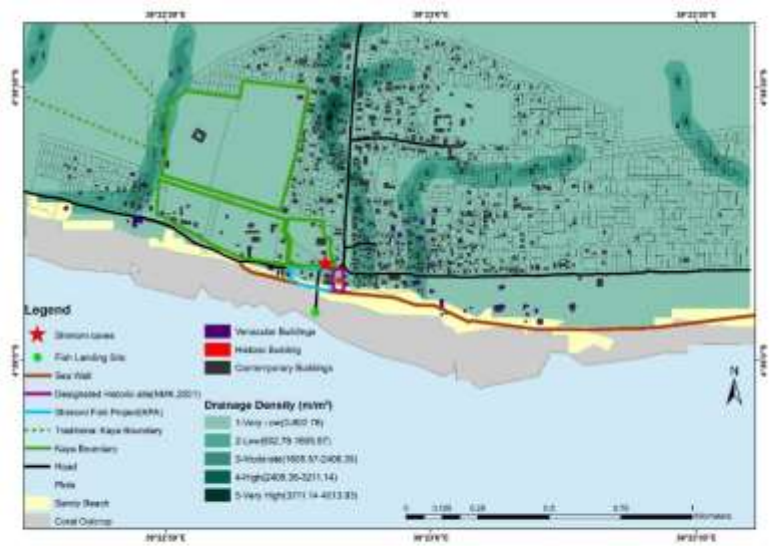

Figure 5: Figure 5: Drainage Density (Source: Authors, 2026)

Where drainage pathways are obstructed, narrowed, or built over, runoff is redirected laterally into cemeteries, ritual grounds and residential compounds that were not originally designed to withstand concentrated flood flows. This finding highlights the relationship between historical settlement morphology and contemporary flood vulnerability. The results therefore demonstrate that drainage density should guide the redesign of drainage channels, ecological buffers, building setbacks, and surface permeability interventions in order to reduce recurrent ponding around culturally sensitive spaces.

The Topographic Wetness Index (TWI) further demonstrated the importance of soil saturation and moisture retention in shaping flood-prone zones. High TWI values ranging from 251.2 to 317.80 covered 12.92 km² (32.20%) of the total study area and contributed 27.41% of total flood risk, whereas low values occupied only 0.44 km² (1.11%) and contributed 3.59% of flood risk (Table 6). Spatially, high wetness zones were concentrated east of the settlement where poor drainage and low infiltration capacity encourage overland flow and prolonged saturation (Figure 6).

Table 6: Topographic Wetness Index

Flood Factor	Subclass	Rank	Remark	Area (km²)	% of Total Area	Flood Area (km²)	% of Flood Area
TWI	0 – 63.8	1	Very Low	0.44	1.11	0.117	3.59
	63.8 – 122.5	2	Low	5.93	14.82	0.55	16.86
	122.5 – 184.7	3	Moderate	8.3	20.75	0.843	25.84
	184.7 – 251.2	4	High	12.41	31.02	0.858	26.3
	251.2 – 317.8	5	Very high	12.92	32.30	0.894	27.41
Total				40	100	3.262	100

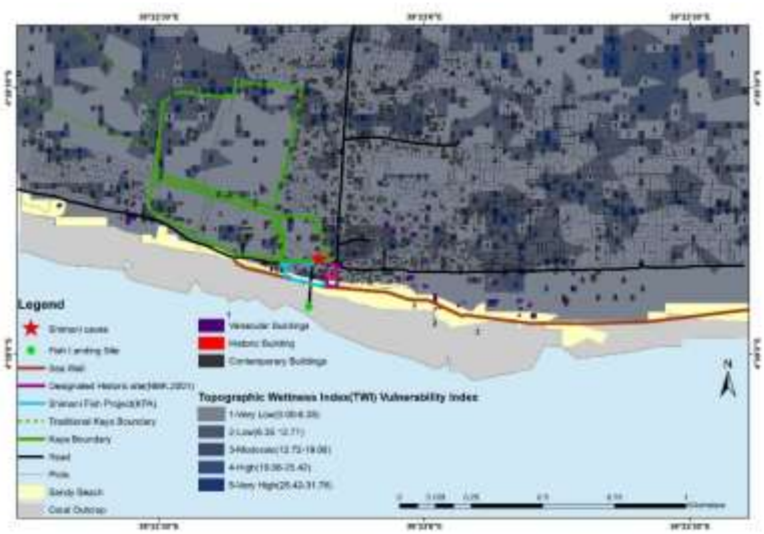

Figure 6: Topographic Wetness Index (Source: Authors, 2026)

Persistent wetness has major implications for the conservation of built heritage because prolonged moisture exposure accelerates deterioration processes within coral stone structures, including salt crystallization, mortar weakening, plaster detachment, and biological colonization. Wetness also affects cemeteries, shrines, and ritual landscapes through waterlogging, grave disturbance, and reduced accessibility. The findings therefore identify high wetness zones as priority conservation-risk areas requiring continuous drainage maintenance, moisture control, and restrictions on incompatible land use and surface sealing.

The Topographic Position Index revealed the influence of relative terrain position on flood susceptibility. Low or negative TPI values ranging from -5.55 to 2.5 occupied 10.5 km² (26.26%) of the study area and contributed 27.34% of flood risk, while high positive values ranging from 4.1 to 5.17 covered 7.14 km² (17.85%) and contributed only 11.92% of flood risk (Table 7). Areas with negative or low values correspond to depressions and lower terrain along the north–south main street where floodwaters accumulate during pluvial flooding events (Figure 7). In contrast, elevated forested areas in the north-east and north-west portions of the settlement exhibited lower flood potential due to improved drainage and runoff dispersion. The analysis demonstrates that relative terrain positioning strongly influences the concentration and persistence of floodwaters within the historic landscape.

Table 7: Topographic Position Index

Flood Factor	Subclass	Rank	Remark	Area (km²)	% of Total Area	Flood Area (km²)	% of Flood Area
TPI	-5.55 – -2.5	5	Very High	10.5	26.26	0.658	27.34
	-2.5 – 0	4	High	10.03	25.08	0.172	7.14
	0 – 2.3	3	Moderate	1.86	4.68	0.691	28.71
	2.3 – 4.1	2	Low	10.47	26.13	0.599	24.89
	4.1 – 5.17	1	Very low	7.14	17.85	0.287	11.92
Total				40	100	2.407	100

From a conservation perspective, the findings reinforce the importance of relative siting analysis in heritage adaptation planning. Historic structures located within local depressions should be prioritized for runoff diversion and drainage enhancement, while elevated zones provide safer locations for visitor infrastructure and future conservation support facilities. Collectively, the hydrological analysis demonstrates that flood vulnerability in historic Shimoni town is strongly shaped by the interaction between runoff concentration, drainage efficiency, moisture retention, and local terrain positioning.

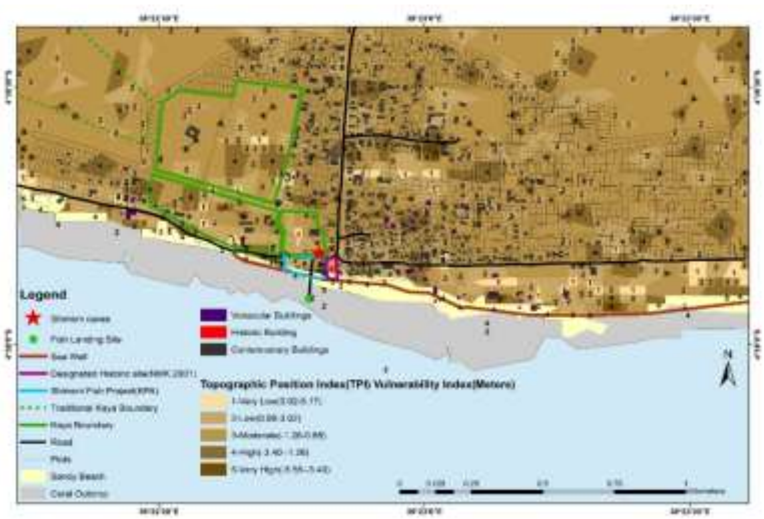

Figure 7: Topographic Position Index (Source:2026)

Surface Condition

The Normalized Difference Vegetation Index (NDVI) significantly influenced flood vulnerability in Shimoni because vegetation affects rainfall infiltration, runoff velocity, and soil stability. Low NDVI values ranging from 0.27 to 0.32 covered 4.9 km² (12.47%) of the study area and contributed 14.93% of total flood risk (Table 8). These sparsely vegetated zones, mainly concentrated along the densely occupied north–south main street, experience increased runoff, reduced infiltration, and higher susceptibility to localized flooding and erosion due to settlement expansion and limited green spaces (Figure 8). In contrast, higher NDVI values ranging from 0.45 to 0.51 occupied 0.09 km² (0.23%) of the study area but contributed 21.67% of flood risk. This indicates that vegetation alone cannot fully offset flooding in low-lying and moistureretaining areas where other topographic and hydrological constraints persist. The findings therefore demonstrate that flood vulnerability in Shimoni is shaped by the interaction between vegetation cover, terrain conditions, and drainage characteristics.

Table 8: Normalized Difference Vegetation Index

Flood Factor	Subclass	Rank	Remark	Area (km²)	% of Total Area	Flood Area (km²)	% of Flood Area
NDVI	0.27 – 0.32	5	Very High	4.99	12.47	0.206	14.93
	0.32 – 0.36	4	High	17.34	43.35	0.130	9.42
	0.36 – 0.4	3	Moderate	6.82	17.05	0.583	42.25
	0.4 – 0.45	2	Low	10.76	26.90	0.162	11.74
	0.45 – 0.51	1	Very low	0.09	0.23	0.299	21.67
Total				40	100	1.38	100

From a heritage conservation perspective, vegetation performs important ecological and cultural functions within sacred groves, cemeteries, ritual grounds, mosque ruins, and colonial coral-stone landscapes. Indigenous vegetation stabilizes soils, slows runoff, reduces erosion, and protects fragile heritage surfaces from moisture-related deterioration. Conversely, vegetation loss increases exposure to runoff and structural decay. The study therefore highlights the need to protect and restore indigenous vegetation buffers around flood-prone heritage sites while regulating settlemnt encroachment within vulnerable areas.

Figure 8: Normalized Difference Vegetation Index (Source: Authors,2026)

Finally, the linear combination approach was used to aggregate the seven flood causative factors into a single flood hazard map of the study area (Figure 9). Findings indicate that high and very high flood-susceptible areas are located along the north-south main street adjacent to the dense wattle-daub settlement and designated historic site comprising of colonial era structures. In contrast, low and very low flood-susceptible areas are located at the periphery of the sacred Kaya forest west of the settlement. Overall, the spatial pattern of high flood susceptibility indicates that heritage spaces considered most vulnerable to flooding include British colonial headquarters, colonial prisons, colonial armouries, cemeteries, mosque ruins, old jetties, and the entry to caves that extend 7 km underground located in the designated historic site

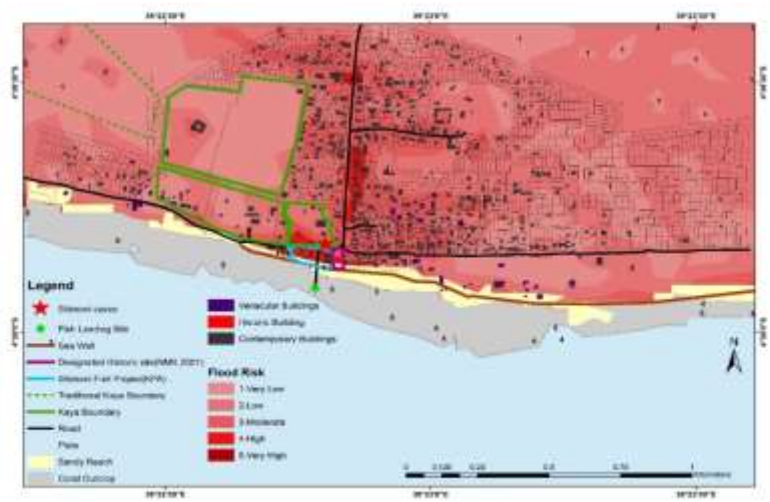

Figure 9: Flood Risk Map of Historic Shimoni Town (Source: Authors,2026)

Spatial Correlation Analysis

The statistical and spatial correlation analysis demonstrates that flood vulnerability in historic Shimoni town is primarily controlled by topographic and hydrological conditions rather than vegetation cover alone. Among all variables, slope emerged as the strongest predictor of flood susceptibility, showing a strong inverse correlation with flooding ($r = -0.84$) (Figure 10). Very gentle slopes (0–2.3°) contributed 44.11% of total flood risk despite occupying only 3.62% of the study area, confirming that flatter terrain promotes prolonged ponding, slower runoff, and increased water retention. Elevation also exhibited a strong negative relationship with flood vulnerability ($r = -0.76$), with low-lying terrain between -5 and 1.8 m contributing 28.82% of flood risk due to runoff concentration and tidal inundation.

Hydrological variables further reinforce this spatial pattern. High drainage density (28.76%), high Topographic Wetness Index values (27.41%), low Topographic Position Index depressions (27.34%), and high flow accumulation zones (26.33%) consistently corresponded with flood-prone eastern and central sections of the settlement. Strong positive correlations between flow accumulation and TWI ($r = 0.74$), drainage density and flow accumulation ($r = 0.69$), indicate significant hydrological interdependence between runoff convergence, prolonged soil saturation, and flood persistence. Similarly, the strong relationship between elevation and TPI ($r = 0.73$) confirms that depressions and low-relief terrain function as primary flood-retention zones.

In contrast, vegetation cover exhibited a comparatively weaker influence on flood vulnerability. NDVI showed only a moderate negative correlation with flooding ($r = -0.42$), indicating that although vegetation enhances infiltration and reduces runoff, it cannot fully offset the effects of unfavorable terrain, poor drainage, and moisture accumulation. Overall, the findings identify slope, elevation, drainage density, TWI, and flow accumulation as the dominant spatial drivers of flood vulnerability in historic Shimoni town, while vegetation acts mainly as a secondary moderating factor.

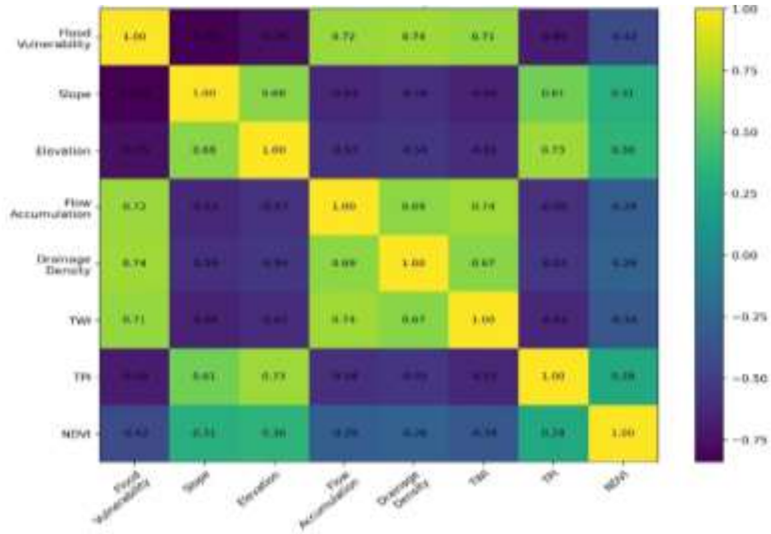

Figure 10: Spatial Correlation Matrix of Flood Vulnerability Factors (Source: Authors,2026)

Discussion

The findings demonstrate that flood vulnerability in historic Shimoni Town is fundamentally shaped by the interaction between topography, hydrology, settlement morphology, and heritage spatial distribution, extending emerging scholarship on climate impacts within maritime cultural landscapes (Taib et al., 2024; Mohammed et al., 2024; Cacciotti et al., 2024; Maou et al., 2025; Allam et al., 2025; Tascón-González et al., 2024; Ashfaq et al., 2025; Haou et al., 2025; Hanwat & Tripathi, 2025). Statistically, slope emerged as the dominant control on flood susceptibility, with very gentle slopes (0–2.3°) contributing 44.11% of total flood risk despite occupying only 3.62% of the area, indicating strong spatial concentration of hazard in low-gradient heritage zones. Low elevations (-5 to 1.8 m) contributed 28.82% of flood risk, while high drainage density (28.76%), high Topographic Wetness Index (27.41%), low Topographic Position Index depressions (27.34%), and high flow accumulation (26.33%) further intensified flood concentration in eastern and central settlement corridors. Notably, higher NDVI values (0.45–0.51), though occupying only 0.09 km² (0.23%), still contributed 21.67% of flood risk, demonstrating that vegetation alone cannot offset structurally constrained hydrological accumulation in low-lying terrain.

Theoretically, the study advances heritage climatology by demonstrating that vulnerability in coastal historic towns is not monument-specific but embedded within coupled geomorphological–hydrological systems. This challenges earlier coastal Kenya studies that primarily emphasized sea-level rise and shoreline erosion (Awuor et al.,2008; Johnson, 2013; Omuombo et al., 2013; Mwakumanya, 2021), by revealing how internal drainage inefficiency, low-relief topography, and settlement pattern jointly drive pluvial flooding within heritage landscapes.

Methodologically, the study represents one of the first DEM-based Flood Hazard Index applications for built heritage in Kenya, extending comparable GIS-based flood mapping approaches in other African contexts (Abbey et al., 2019; Osman & Das, 2023; Khalil et al., 2022; Maou et al., 2025; Allam et al., 2025) by explicitly linking hydrological variables to heritage asset distribution, including colonial, ritual, and sacred sites.

From a policy and practice perspective, the results provide an operational spatial framework for integrating climate adaptation within the National Museums and Heritage Act, Kenya National Adaptation Plan 2015–2030, National Climate Change Action Plan 2027–2030, Physical and Land Use Planning Act 2019, Integrated Coastal Zone Management Plan 2019–2023, and Kwale County Spatial Plan 2022–2032. The mixed NDVI response, where low vegetation areas contributed 14.93% of flood risk while higher vegetation zones still recorded 21.67%, further confirms that ecological cover alone is insufficient without concurrent drainage and terrain-sensitive interventions. Consequently, effective adaptation requires a shift toward landscape-scale strategies integrating watershed management, runoff attenuation, ecological buffering, heritage-sensitive zoning, and redesigned drainage systems for climate-vulnerable historic settlements.

Conclusion

Flood vulnerability in historic Shimoni Town is spatially concentrated and primarily governed by interacting topographic, hydrological, and settlement structure controls. Flood risk is strongly concentrated in low-lying and low-gradient areas, with very gentle slopes (0–2.3°) contributing 44.11% of flood risk despite covering only 3.62% of the area, and low elevations (-5 to 1.8 m) contributing 28.82%. Hydrological factors including high drainage density (28.76%), TWI (27.41%), low TPI depressions (27.34%), and high flow accumulation (26.33%), further intensify runoff concentration in eastern and central corridors. Even higher NDVI zones (0.45–0.51), though spatially limited (0.23%), contribute 21.67% of flood risk, showing that vegetation alone cannot offset terrain-driven hydrological accumulation. Overall, results indicate a shift from isolated hotspots to broader hydrology–heritage system interactions concentrated along drainage pathways and shoreline margins.

Critically, the study shows that flood vulnerability extends beyond individual monuments to interconnected cultural landscapes where access routes, settlement expansion, and drainage modification amplify exposure of colonial structures, sacred sites, cemeteries, jetties, and ritual caves. This systemic coupling suggests that future climate change, sea level rise, and land-use intensification will likely accelerate both physical deterioration and functional loss of heritage landscapes if unmanaged.

From a policy perspective, the findings support a transition toward landscape-scale and watershed-based heritage governance, integrating flood zoning, drainage redesign, runoff attenuation, ecological restoration, and controlled development within retention zones. The limited buffering effect of vegetation further underscores the need for combined geomorphological and planning interventions rather than isolated ecological solutions. Importantly, the framework is scalable and transferable to other coastal and archipelagic heritage systems facing similar hydrological constraints. Overall, this study advances heritage climatology by demonstrating that flood risk in coastal historic towns is a structurally embedded landscape phenomenon, requiring integrated, cross-sectoral, and spatially explicit adaptation strategies that reposition heritage conservation within broader climate resilience and land-use governance systems.

Recommendations

Flood adaptation in historic Shimoni Town should prioritize spatially identified high-risk zones, particularly low-lying eastern and central areas where very gentle slopes (44.11% of flood risk), low elevations (28.82%), high drainage density (28.76%), high TWI (27.41%), low TPI depressions (27.34%), and high flow accumulation (26.33%) jointly concentrate flood hazards. These statistically defined hotspots provide a clear basis for targeting interventions.

Short-Term Site-Level Actions

Short-term, site-level actions should focus on rapid drainage improvement and protection of vulnerable heritage assets in flood-retention corridors. Measures such as contour drains, vegetated swales, permeable paving, infiltration strips, and localized runoff diversion should be prioritized along the north–south main street, shoreline depressions, and around colonial buildings, mosque ruins, cemeteries, ritual caves, and jetties. These interventions are low-cost and highly feasible and can be implemented through coordination between the National Museums of Kenya (NMK), National Environment Management Authority (NEMA), and Kwale County Government under the, Kenya National Adaptation Plan 2015–2030.

A complementary short-term priority is the establishment of flood monitoring and early warning systems in high-flow accumulation and high-wetness zones. Installation of rainfall gauges, groundwater monitoring points, and community-based alert systems, coordinated with the Kenya Meteorological Department (KMD), would strengthen preparedness and response capacity.

Long-Term Site-Level Strategies

Long-term, site-level strategies should emphasize ecological restoration and planned relocation. Given that low NDVI areas contribute 14.93% of flood risk, restoration of vegetation buffers around sacred groves, cemeteries, and shoreline corridors should be expanded through Kenya Forest Service and community forest associations. However, because vegetation alone is insufficient against structurally driven flooding, these measures must be integrated with drainage redesign. In persistently flooded low TPI zones (27.34%), selective relocation of vulnerable functions and restrictions on new development are necessary under the Physical and Land Use Planning Act 2019 and Kwale County Spatial Plan 2022–2032.

Policy-Level Implications

Policy-level implications include mainstreaming DEM-based Flood Hazard Index outputs into heritage conservation approvals, urban planning, and marine spatial governance under the Environmental Management and Coordination Act 2015. Flood risk in Shimoni reflects a broader hydrology–heritage system, requiring watershed-scale zoning, drainage setbacks, and integration of shoreline and mangrove management into marine spatial planning. Overall, the study supports a shift from monument-centered conservation to scalable, landscape-based climate adaptation, providing a transferable framework for other vulnerable coastal heritage towns.

Disclosure Statement

The authors report no competing interests to declare.

Funding Details

No funding was received for this study.

References

Abay, A., Barbieri, G., & Woldearegay, K. (2019). GIS-based landslide susceptibility evaluation using the analytical hierarchy process (AHP) approach: The case of Tarmaber District, Ethiopia. *Momona Ethiopian Journal of Science, 11*(1), 14. https://doi.org/10.4314/mejs.v11i1.2

Adnan, M. S. G., Dewan, A., Zannat, K. E., & Abdullah, A. Y. M. (2019). The use of watershed geomorphic data for flash-flood susceptibility zoning: A case study of the Karnaphuli and Sangu river basins of Bangladesh. *Natural Hazards, 99*(1), 425–448. https://doi.org/10.1007/s11069-019-03749-3

Ahmad, R., Maulud, K. N. A., Zamir, U. B., Razali, S. F. M., Yaseen, Z. M., Pradhan, B., Khan, M. N., & Eshquvvatov, B. (2025). A systematic literature review of digital elevation models and hydrological models integration for advanced flood risk management. *Geomatics, Natural Hazards and Risk, 16*(1). https://doi.org/10.1080/19475705.2025.2549487

Alafostergios, N., Evelpidou, N., & Spyrou, E. (2025). Flood susceptibility assessment based on the analytical hierarchy process (AHP) and geographic information systems (GIS): A case study of the broader area of Megala Kalyvia, Thessaly, Greece. *Information, 16*(8), 671. https://doi.org/10.3390/info16080671

Alba-Fernández, M. V., Ariza-López, F. J., & Jiménez-Gamero, M. D. (2021). A new approach to the quality control of slope and aspect classes derived from digital elevation models. *Remote Sensing, 13*(11), 2069. https://doi.org/10.3390/rs13112069

Allam, A. M., Ibrahim, M. G., Kanae, S., & Sharaan, M. (2025). Evaluating flood and landslide hazards to cultural heritage sites in Historic Cairo. *Natural Hazards, 121*(13), 15491–15535. https://doi.org/10.1007/s11069-025-07401-1

Alqahtani, F., & Qaddah, A. A. (2019). GIS digital mapping of flood hazard in Jeddah–Makkah region from morphometric analysis. *Arabian Journal of Geosciences, 12*(6). https://doi.org/10.1007/s12517-019-4338-8

Al-Sababhah, N. (2023). Topographic position index to landform classification and spatial planning, using GIS, for Wadi Araba, South West Jordan. *Environment and Ecology Research, 11*(1), 79–101. https://doi.org/10.13189/eer.2023.110106

Amellah, O., Mignosa, P., Prost, F., & Aureli, F. (2024). Assessment of flood hazard mapping using a DEM-based approach and 2D hydrodynamic modeling. *Water, 16*(13), 1844. https://doi.org/10.3390/w16131844

Appiotti, F., Assumma, V., Bottero, M., Campostrini, P., Datola, G., Lombardi, P., & Rinaldi, E. (2020). Definition of a risk assessment model within a European interoperable database platform (EID) for cultural heritage. *Journal of Cultural Heritage, 46*, 268–277. https://doi.org/10.1016/j.culher.2020.08.001

Arrighi, C. (2021). A global scale analysis of river flood risk of UNESCO World Heritage Sites. *Frontiers in Water, 3*. https://doi.org/10.3389/frwa.2021.764459

Ashfaq, S., Tufail, M., Niaz, A., Muhammad, S., Alzahrani, H., & Tariq, A. (2025). Flood susceptibility assessment and mapping using GIS-based analytical hierarchy process and frequency ratio models. *Global and Planetary Change, 251*, 104831. https://doi.org/10.1016/j.gloplacha.2025.104831

Asrade, T. M., Abebe, S. A., Tadesse, K. B., Kerebih, M. S., & Meshesha, T. M. (2026). Flood susceptibility assessment using three machine learning techniques and comparison of their performance. *Scientific Reports, 16*(1). https://doi.org/10.1038/s41598-026-38391-0

Awuor, C. B., Orindi, V. A., & Adwera, A. O. (2008). Climate change and coastal cities: The case of Mombasa, Kenya. *Environment and Urbanization, 20*(1), 231–242. https://doi.org/10.1177/0956247808089158

Bashir, B. (2023). Morphometric parameters and geospatial analysis for flash flood susceptibility assessment: A case study of Jeddah City along the Red Sea Coast, Saudi Arabia. *Water, 15*(5), 870. https://doi.org/10.3390/w15050870

Basu, T., Mondal, B. K., Abdelrahman, K., Fnais, M. S., & Praharaj, S. (2023). Assessing urban flood hazard vulnerability using multi-criteria decision making and geospatial techniques in Nabadwip Municipality, West Bengal, India. *Atmosphere, 14*(4), 669. https://doi.org/10.3390/atmos14040669

Bello, M., Singh, S., Singh, S. K., Pandey, V., Kumar, P., Meraj, G., Kanga, S., & Sajan, B. (2024). Geospatial analysis of flood susceptibility in Nigeria's vulnerable coastal states: A detailed assessment and mitigation strategy proposal. *Climate, 12*(7), 93. https://doi.org/10.3390/cli12070093

Betts, J., Young, R. P., Hilton-Taylor, C., Hoffmann, M., Rodríguez, J. P., Stuart, S. N., & Milner-Gulland, E. J. (2019). A framework for evaluating the impact of the IUCN Red List of threatened species. *Conservation Biology, 34*(3), 632–643. https://doi.org/10.1111/cobi.13454

Bishikwabo, I., Mambo, H., Kamanda, J. K., Abdelbaki, C., Nanyunga, M. A., & Kumar, N. (2025). Urban flood susceptibility mapping using GIS and the analytical hierarchy process: Case of the City of Uvira, Democratic Republic of the Congo. *GeoHazards, 6*(3), 38. https://doi.org/10.3390/geohazards6030038

Blavier, C. L. S., Huerto-Cardenas, H. E., Aste, N., Del Pero, C., Leonforte, F., & Della Torre, S. (2023). Adaptive measures for preserving heritage buildings in the face of climate change: A review. *Building and Environment, 245*, 110832. https://doi.org/10.1016/j.buildenv.2023.110832

Bonazza, A., & Sardella, A. (2023). Climate change and cultural heritage: Methods and approaches for damage and risk assessment addressed to a practical application. *Heritage, 6*(4), 3578–3589. https://doi.org/10.3390/heritage6040190

Boulton, S. J., & Stokes, M. (2018). Which DEM is best for analysing fluvial landscape development in mountainous terrains? *Geomorphology, 310*, 168–187. https://doi.org/10.1016/j.geomorph.2018.03.002

Brimblecombe, P., & Richards, J. (2024). Applied climatology for heritage. *Theoretical and Applied Climatology, 155*(8), 7325–7333. https://doi.org/10.1007/s00704-024-05059-6

Burshtynska, K., Zayats, I., Halochkin, M., Bakuła, K., & Babiy, L. (2023). The influence of the main factors on the accuracy of hydrological modelling of flooded lands. *Water, 15*(18), 3303. https://doi.org/10.3390/w15183303

Busaka, B. M., Akalla, J. A., & Ngari, L. K. (2023). Conservation and preservation of immovable heritage from below: Local community involvement in the management of Shimoni Caves in the South Coast of Kenya. *The International Journal of Humanities & Social Studies*. https://doi.org/10.24940/theijhss/2023/v11/i7/hs2307-021

Cacciotti, R., Sardella, A., Drdácký, M., & Bonazza, A. (2024). A methodology for vulnerability assessment of cultural heritage in extreme climate change. *International Journal of Disaster Risk Science, 15*(3), 404–420. https://doi.org/10.1007/s13753-024-00564-8

Cazalis, V., Di Marco, M., Butchart, S. H. M., Akçakaya, H. R., González-Suárez, M., Meyer, C., et al. (2022). Bridging the research–implementation gap in IUCN Red List assessments. *Trends in Ecology & Evolution, 37*(4), 359–370. https://doi.org/10.1016/j.tree.2021.12.002

Cece Siago. (2024, March 26). Concern as high tides send ocean water into villages. *The Nation*. https://nation.africa/kenya/counties/kwale/concern-as-high-tides-send-ocean-water-into-villages--4588866

Chowdhury, M. S. (2023). Modelling hydrological factors from DEM using GIS. *Methods, 10*, 102062. https://doi.org/10.1016/j.mex.2023.102062

Cook, I., Johnston, R., & Selby, K. (2019). Climate change and cultural heritage: A landscape vulnerability framework. *The Journal of Island and Coastal Archaeology, 16*(2–4), 553–571. https://doi.org/10.1080/15564894.2019.1605430

Devi, K., Reddy, C. C., Rahul, K., Khuntia, J. R., & Das, B. S. (2025). A holistic methodology for evaluating flood vulnerability, generating a flood risk map, and conducting a detailed flood inundation assessment. *Scientific Reports, 15*(1), 28253. https://doi.org/10.1038/s41598-025-13025-z

Dragičević, N., Karleuša, B., & Ožanić, N. (2019). Different approaches to estimating drainage density and their effects on the erosion potential method. *Water, 11*(3), 593. https://doi.org/10.3390/w11030593

Elsebaie, I. H., Kawara, A. Q., & Alnahit, A. O. (2023). Mapping and assessment of flood risk in the Wadi Al-Lith Basin, Saudi Arabia. *Water, 15*(5), 902. https://doi.org/10.3390/w15050902

Gao, H., Liu, F., Yan, T., Qin, L., & Li, Z. (2022). Drainage density and its controlling factors on the eastern margin of the Qinghai–Tibet Plateau. *Frontiers in Earth Science, 9*. https://doi.org/10.3389/feart.2021.755197

Gitau, D. K., Wahome, E. W., Njuguna, B. M., & Abuje, S. J. (2025). The conservation imperative: Developing a framework for climate change adaptation in coastal heritage conservation—A study of monuments in Kenya. *American Journal of Climate Change, 14*(03), 437–458. https://doi.org/10.4236/ajcc.2025.143022

Government of Kenya. (2019). *Integrated Coastal Zone Action Plan for Kenya (2019-2023)*. National Environment Management Authority (NEMA).

Guth, P. L., Van Niekerk, A., Grothmann, C. H., Muller, J., Hawker, L., Florinsky, I. V., Gesch, D., Reuter, H. I., Herrera-Cruz, V., Riazanoff, S., López-Vázquez, C., Carabajal, C. C., Albinet, C., & Strobl, P. (2021). Digital elevation models: Terminology and definitions. *Remote Sensing, 13*(18), 3581. https://doi.org/10.3390/rs13183581

Habib, M. (2021). Quantifying topographic ruggedness using principal component analysis. *Advances in Civil Engineering, 2021*(1). https://doi.org/10.1155/2021/3311912

Hamza, A. J., Esteves, L. S., Cvitanovic, M., & Kairo, J. (2020). Past and present utilization of mangrove resources in Eastern Africa and drivers of change. *Journal of Coastal Research, 95*(sp1), 39. https://doi.org/10.2112/si95-008.1

Hanwat, S., & Tripathi, V. K. (2025). Flood risk using GIS-based MCDA approach for a case study. *Water Practice & Technology, 21*(1), 284–312. https://doi.org/10.2166/wpt.2025.171

Haou, M. E., Ourribane, M., Ismaili, M., Abdelrahman, K., Fnais, M. S., Krimissa, S., Oudi, H. E., Hajji, S., Bouzkraoui, M. E., Tarchi, F., & Namous, M. (2025). Advanced GIS-based modeling for flood hazards mapping in urban semi-arid regions: Insights from Beni Mellal, Morocco. *Frontiers in Environmental Science, 13*. https://doi.org/10.3389/fenvs.2025.1585926

Ikirri, M., Faik, F., Echogdali, F. Z., Antunes, I. M. H. R., Abioui, M., Abdelrahman, K., Fnais, M. S., Wanaim, A., Id-Belqas, M., Boutaleb, S., Sajinkumar, K. S., & Quesada-Román, A. (2022). Flood hazard index application in arid catchments: Case of the Taguenit Wadi Watershed, Lakhssas, Morocco. *Land, 11*(8), 1178. https://doi.org/10.3390/land11081178

Iosub, M. (2019). Flash flood impact on the cultural heritage in Moldova Region, Romania. Case study: Jijia Valley. *International Multidisciplinary Scientific GeoConference SGEM*. https://doi.org/10.5593/sgem2019/2.2/s11.103

Jiang, W., Yu, J., Wang, Q., & Yue, Q. (2022). Understanding the effects of digital elevation model resolution and building treatment for urban flood modelling. *Journal of Hydrology: Regional Studies, 42*, 101122. https://doi.org/10.1016/j.ejrh.2022.101122

Johnson, U. K. (2013). River sediment supply, sedimentation and transport of the highly turbid sediment plume in Malindi Bay, Kenya. *Journal of Geographical Sciences, 23*(3), 465–489. https://doi.org/10.1007/s11442-013-1022-x

Kazungu Kalume. (2020, May 26). Over 600 families in the cold as floods hit villages in Lamu. *Daily Nation*. https://reliefweb.int/report/kenya/over-600-families-cold-floods-hit-villages-lamu

Kazungu Kalume. (2024, August 31). Concerns raised over frequent destruction of Coast seawall. *Daily Nation*. https://nation.africa/kenya/counties/lamu/concerns-raised-over-frequent-destruction-of-coast-seawall-4745096

Khalifa, A., Bashir, B., Alsalman, A., & Bachir, H. (2022). Morphometric-hydro characterization of the coastal line between El-Qussier and Marsa-Alam, Egypt: Preliminary flood risk signatures. *Applied Sciences, 12*(12), 6264. https://doi.org/10.3390/app12126264

Khalil, M. M. E., Khodary, S. M., Youssef, Y. M., Alsubaie, M. S., & Sallam, A. (2022). Geo-environmental hazard assessment of archaeological sites and archaeological domes—Fatimid tombs—Aswan, Egypt. *Buildings, 12*(12), 2175. https://doi.org/10.3390/buildings12122175

Kilaka, B. M., & De Jesus Neto, A. G. (2023). The "Lamu Port-South Sudan-Ethiopia" Transport Corridor (LAPSSET): Contradictions of a circulation mega project in contemporary East Africa. An interview with Benard Musembi Kilaka. *Boletim GeoÁfrica, 2*(6), 6–13. https://doi.org/10.59508/geoafrica.v2i6.59838

Kiriama, H. O. (2017). Memory, identity and heritage in the South Coast of Kenya: Case of Shimoni Slave Caves. *Journal of African Cultural Heritage Studies, 1*(1), 4. https://doi.org/10.22599/jachs.10

Kopecký, M., Macek, M., & Wild, J. (2020). Topographic Wetness Index calculation guidelines based on measured soil moisture and plant species composition. *Science of the Total Environment, 757*, 143785. https://doi.org/10.1016/j.scitotenv.2020.143785

Kotova, L., Leissner, J., Winkler, M., Kilian, R., Bichlmair, S., Antretter, F., Moßgraber, J., Reuter, J., Hellmund, T., Matheja, K., Rohde, M., & Mikolajewicz, U. (2023). Making use of climate information for sustainable preservation of cultural heritage: Applications to the KERES project. *Heritage Science, 11*(1). https://doi.org/10.1186/s40494-022-00853-9

Kusimba, C. M. (2004). Archaeology of slavery in East Africa. *African Archaeological Review, 21*(2), 59–88. https://doi.org/10.1023/b:aarr.0000030785.72144.4a

Lee, S., & Rezaie, F. (2022). Data used for GIS-based flood susceptibility mapping. *GEO DATA, 4*(1), 1–15. https://doi.org/10.22761/dj2022.4.1.001

Liang, W., & Chan, M. (2017). Spatial and temporal variations in the effects of soil depth and topographic wetness index of bedrock topography on subsurface saturation generation in a steep natural forested headwater catchment. *Journal of Hydrology, 546*, 405–418. https://doi.org/10.1016/j.jhydrol.2017.01.033

Mabrouk, M. M. S., Abdel-Salam, E. M. W., & Serwa, A. (2022). Geomorphological hazard analysis using DEM along the Eastern coast between Marsa Alam and Ras Gharib, Egypt. *Engineering Research Journal, 174*(0), 1–21. https://doi.org/10.21608/erj.2022.240856

Maou, A., Souadnia, S., Faqeih, K., AlAmri, A., Hadji, R., Alamri, S. M., Harizi, K., Alamery, E., Sonia, G., Leila, B., & Altwaiher, J. (2025). Assessing flash-flood occurrences and hazard zones along the Mediterranean coasts: A GIS and mapping-techniques approach in the Wadi Saf Saf Basin, Northeast Algeria. *Frontiers in Earth Science, 13*. https://doi.org/10.3389/feart.2025.1594364

Mishra, B. P., Ghose, D. K., & Satapathy, D. P. (2022). Geospatial modeling using a hybrid machine learning approach for flood susceptibility. *Earth Science Informatics, 15*(4), 2619–2636. https://doi.org/10.1007/s12145-022-00872-x

Mohammed, Z. T., Hussein, L. Y., & Abood, M. H. (2024). Potential flood hazard mapping based on GIS and the analytical hierarchy process. *Journal of Water Management Modeling*. https://doi.org/10.14796/jwmm.c528

Mwakumanya, M. A. (2021). Beach erosion hazard vulnerability assessment of Bamburi Beach in Mombasa, Kenya. *International Journal of Environmental Science and Development, 12*(3), 80–86. https://doi.org/10.18178/ijesd.2021.12.3.1322

Neoga, N., Victoria, M. F., Salman, H., & Oyetunji, A. K. (2025). Integrating GIS into flood risk management: A Global South perspective on resilience, planning, and policy. *Water, 17*(21), 3149. https://doi.org/10.3390/w17213149

Neto, N. G., & Carr, C. A. (2021). The source of terrain slope data is an important consideration for natural resource management: A comparison of field-measured and DEM-calculated slope values. *Rangelands, 43*(3), 111–116. https://doi.org/10.1016/j.rala.2020.12.005

Njiiri, W., Njuguna, M., & Wahome, E. (2024). Determination of shoreline variability for adaptation of maritime built heritage to climate change: A case of Southern Kenya Coast. *The Historic Environment: Policy & Practice, 15*(4), 594–610. https://doi.org/10.1080/17567505.2024.2435083

Njiiri, W., Njuguna, M., & Wahome, E. (2025). Establishing climate variability for adaptation of maritime cultural and natural heritage to climate change in the South Coast, Kenya. *Journal of the Kenya National Commission for UNESCO*. https://doi.org/10.62049/jkncu.v5i1.405

Njiiri, W., Njuguna, M., & Wahome, E. (2025a). Establishing historical shoreline trends for adaptation of maritime built heritage to climate change, Part 2: The Northern Kenya Coast. *The Historic Environment: Policy & Practice, 16*(1), 167–186. https://doi.org/10.1080/17567505.2025.2470475

Omuombo, C. A., Olago, D. O., & Odada, E. O. (2013). Coastal erosion. In *Developments in Earth Surface Processes* (pp. 331–339). https://doi.org/10.1016/b978-0-444-59559-1.00022-0

Osman, S. A., & Das, J. (2023). GIS-based flood risk assessment using multi-criteria decision analysis of the Shebelle River Basin in southern Somalia. *SN Applied Sciences, 5*(5). https://doi.org/10.1007/s42452-023-05360-5

Oyugi, M. O. (2021). Urbanisation footprints and the distribution of air quality in Nairobi City, Kenya. *Journal of Environmental & Earth Sciences, 3*(2), 14–44. https://doi.org/10.30564/jees.v3i2.3289

Pimenta, L., Duarte, L., Teodoro, A. C., Beltrão, N., Gomes, D., & Oliveira, R. (2025). GIS-based flood susceptibility mapping using AHP in the Urban Amazon: A case study of Ananindeua, Brazil. *Land, 14*(8), 1543. https://doi.org/10.3390/land14081543

Reimann, L., Vafeidis, A. T., Brown, S., Hinkel, J., & Tol, R. S. J. (2018). Mediterranean UNESCO World Heritage at risk from coastal flooding and erosion due to sea-level rise. *Nature Communications, 9*(1), 4161. https://doi.org/10.1038/s41467-018-06645-9

Różycka, M., Migoń, P., & Michniewicz, A. (2017). Topographic Wetness Index and Terrain Ruggedness Index in the geomorphic characterization of landslide terrains: Examples from the Sudetes, SW Poland. *Zeitschrift Für Geomorphologie, 61*(2), 61–80. https://doi.org/10.1127/zfg_suppl/2016/0328

Sajid, T., Maimoon, S. K., Waseem, M., Ahmed, S., Khan, M. A., Tränckner, J., Pasha, G. A., Hamidifar, H., & Skoulikaris, C. (2025). Integrated risk assessment of floods and landslides in Kohistan, Pakistan. *Sustainability, 17*(8), 3331. https://doi.org/10.3390/su17083331

Salazar, L. G. F., Figueiredo, R., & Romão, X. (2024). Flood vulnerability assessment of built cultural heritage: A literature review and indicator identification. *International Journal of Disaster Risk Reduction, 111*, 104666. https://doi.org/10.1016/j.ijdrr.2024.104666

Saranya, J. S., Roxy, M. K., Dasgupta, P., & Anand, A. (2022). Genesis and trends in marine heatwaves over the tropical Indian Ocean and their interaction with the Indian summer monsoon. *Journal of Geophysical Research: Oceans, 127*(2). https://doi.org/10.1029/2021jc017427

Sesana, E., Gagnon, A. S., Bonazza, A., & Hughes, J. J. (2019). An integrated approach for assessing the vulnerability of World Heritage Sites to climate change impacts. *Journal of Cultural Heritage, 41*, 211–224. https://doi.org/10.1016/j.culher.2019.06.013

Shrestha, S., Dahal, D., Poudel, B., Banjara, M., & Kalra, A. (2025). Flood susceptibility analysis with integrated geographic information system and analytical hierarchy process: A multi-criteria framework for risk assessment and mitigation. *Water, 17*(7), 937. https://doi.org/10.3390/w17070937

Shuaibu, A., Hounkpè, J., Bossa, Y. A., & Kalin, R. M. (2022). Flood risk assessment and mapping in the Hadejia River Basin, Nigeria, using the hydro-geomorphic approach and the multi-criterion decision-making method. *Water, 14*(22), 3709. https://doi.org/10.3390/w14223709

Slezák, M., Douda, J., Šibíková, M., Jarolímek, I., Senko, D., & Hrivnák, R. (2022). Topographic indices predict the diversity of Red List and non-native plant species in human-altered riparian ecosystems. *Ecological Indicators, 139*, 108949. https://doi.org/10.1016/j.ecolind.2022.108949

Taib, H., Hadji, R., Bedri, K., Defaflia, N., Hamed, Y., Gentilucci, M., Barbieri, M., & Pambianchi, G. (2024). Morphometric analysis and risk assessment of flash floods in the Atlas chain of eastern Algeria and the Algerian–Tunisian borders. *Euro-Mediterranean Journal for Environmental Integration, 10*(2), 749–763. https://doi.org/10.1007/s41207-024-00617-w

Tanrıverdi, M., & Ayaşlıgil, T. E. (2026). From expert-based evaluation to data-driven modeling: Performance-based flood susceptibility mapping. *Limnological Review, 26*(1), 6. https://doi.org/10.3390/limnolrev26010006

Tascón-González, L., Ferrer-Julià, M., & García-Meléndez, E. (2024). Methodological approach for mapping the flood physical vulnerability index using open-source geographical data: An example in a small- to medium-sized city (Ponferrada, Spain). *Natural Hazards, 120*(5), 4053–4081. https://doi.org/10.1007/s11069-023-06370-7

Tran, T., Nguyen, B. Q., Vo, N. D., Le, M., Nguyen, Q., Lakshmi, V., & Bolten, J. D. (2022). Quantification of global Digital Elevation Model (DEM) – A case study of the newly released

NASADEM for a river basin in Central Vietnam. *Journal of Hydrology: Regional Studies, 45*, 101282. https://doi.org/10.1016/j.ejrh.2022.101282

Wahba, M., Hassan, H. S., Elsadek, W. M., Kanae, S., & Sharaan, M. (2023). Novel utilization of simulated runoff as a causative parameter to predict the hazard of flash floods. *Environmental Earth Sciences, 82*(13). https://doi.org/10.1007/s12665-023-11007-w

Wainwright, C. M., Marsham, J. H., Keane, R. J., Rowell, D. P., Finney, D. L., Black, E., & Allan, R. P. (2019). 'Eastern African Paradox' rainfall decline due to shorter, not less intense, Long Rains. *npj Climate and Atmospheric Science, 2*(1). https://doi.org/10.1038/s41612-019-0091-7

Xafoulis, N., Kontos, Y., Farsirotou, E., Kotsopoulos, S., Perifanos, K., Alamanis, N., Dedousis, D., & Katsifarakis, K. (2023). Evaluation of various resolution DEMs in flood risk assessment and practical rules for flood mapping in data-scarce geospatial areas: A case study in Thessaly, Greece. *Hydrology, 10*(4), 91. https://doi.org/10.3390/hydrology10040091

Xiong, Y., & Wang, H. (2022). Spatial relationships between NDVI and topographic factors at multiple scales in a watershed of the Minjiang River, China. *Ecological Informatics, 69*, 101617. https://doi.org/10.1016/j.ecoinf.2022.101617

Xu, D., Chen, B., Shen, B., Wang, X., Yan, Y., Xu, L., & Xin, X. (2018). The classification of grassland types based on object-based image analysis with multisource data. *Rangeland Ecology & Management, 72*(2), 318–326. https://doi.org/10.1016/j.rama.2018.11.007

Zhang, H., Loáiciga, H. A., Feng, L., He, J., & Du, Q. (2021). Setting the flow accumulation threshold based on environmental and morphologic features to extract river networks from digital elevation models. *ISPRS International Journal of Geo-Information, 10*(3), 186. https://doi.org/10.3390/ijgi10030186

Zhang, J., Cheng, Y., Ge, W., Li, S., He, Q., & Zhang, T. (2025). Quantifying the mixed uncertainty for calculating slope from a gridded digital elevation model. *Geocarto International, 40*(1). https://doi.org/10.1080/10106049.2025.2480307

Zhang, X., & Liu, M. (2022). Topography regulates the responses of water partitioning to climate and vegetation seasonality. *Science of the Total Environment, 838*(Pt 2), 156028. https://doi.org/10.1016/j.scitotenv.2022.156028

Zhao, X., Wu, Z., & Lu, J. (2026). Flood risk assessment and watershed resilience strategies in the Qinba Mountains based on Random Forest and frequency ratio-Borda count analysis. *Geocarto International, 41*(1). https://doi.org/10.1080/10106049.2025.2562549